

A methanotrophic bacterium to enable methane removal for climate mitigation

Lian He^a, Joseph D. Groom^{a,1}, Erin H. Wilson^b, Janette Fernandez^c, Michael C. Konopka^c, David A. C. Beck^{a,d}, and Mary E. Lidstrom^{a,e,2}

Contributed by Mary E. Lidstrom; received June 14, 2023; accepted July 19, 2023; reviewed by James G. Ferry and Jeremy D. Semrau

The rapid increase of the potent greenhouse gas methane in the atmosphere creates great urgency to develop and deploy technologies for methane mitigation. One approach to removing methane is to use bacteria for which methane is their carbon and energy source (methanotrophs). Such bacteria naturally convert methane to CO₂ and biomass, a value-added product and a cobenefit of methane removal. Typically, methanotrophs grow best at around 5,000 to 10,000 ppm methane, but methane in the atmosphere is 1.9 ppm. Air above emission sites such as landfills, anaerobic digestor effluents, rice paddy effluents, and oil and gas wells contains elevated methane in the 500 ppm range. If such sites are targeted for methane removal, technology harnessing aerobic methanotroph metabolism has the potential to become economically and environmentally viable. The first step in developing such methane removal technology is to identify methanotrophs with enhanced ability to grow and consume methane at 500 ppm and lower. We report here that some existing methanotrophic strains grow well at 500 ppm methane, and one of them, Methylotuvimicrobium buryatense 5GB1C, consumes such low methane at enhanced rates compared to previously published values. Analyses of bioreactor-based performance and RNAseq-based transcriptomics suggest that this ability to utilize low methane is based at least in part on extremely low non-growth-associated maintenance energy and on high methane specific affinity. This bacterium is a candidate to develop technology for methane removal at emission sites. If appropriately scaled, such technology has the potential to slow global warming by 2050.

methanotroph \mid specific affinity \mid whole-cell K_M \mid transcriptomics \mid climate change

Methane is a potent greenhouse gas and has a global warming potential over 85 times greater than carbon dioxide (CO_2) on a 20-y timescale (1, 2). Atmospheric methane has been rising quickly in the past 15 y (3) and currently accounts for about 30% of total global warming (4), prompting interest in methane removal technologies (5–8). Methane has an atmospheric lifetime of ~12 y (4), which presents an opportunity for slowing the progress of global warming in the near term if methane removal technologies are promptly deployed (5, 7). Recent projections predict that global warming can be reduced 0.21 to 0.22 °C by removing 0.3 to 1 petagrams methane by 2050 (1, 5). Temperature decreases of this magnitude are predicted to be significant (1, 5), especially when combined with other mitigation strategies (9).

Most proposed methane mitigation solutions are focused on decreasing emissions (5), and these are important goals. However, not all methane emissions are amenable to reduction, and it has been argued that emission reduction strategies must be augmented by methane removal to slow global warming by 2050 (6–8). In addition, any emission reduction strategies that enhance aerobic methanotrophic activity in natural communities may also result in increased nitrous oxide (N_2O) emission, as demonstrated for rice paddy communities in which N_2O reduction by denitrifiers is inhibited by stimulation of aerobic methanotrophs due to competition for copper (10). Since N_2O is ten times more potent as a greenhouse gas than methane (2), any technology for methane mitigation must ensure that it also results in negligible increase in N_2O emissions.

One potential methane mitigation solution is to employ aerobic methanotrophic bacteria, which are capable of assimilating methane naturally at ambient temperature without producing N_2O . Two major challenges exist for such methane removal, low concentration and enormous scale. Atmospheric methane is currently at 1.9 ppm (3), a concentration that makes it difficult for aerobic methanotrophs to survive. Although a methanotroph has been described that grows at atmospheric methane, it apparently cometabolizes CO and H_2 to survive (11). The very low rates of methane consumption at 1.9 ppm create significant challenges for reaching the 0.3 to 1 petagram scale noted above. An alternative is to focus on major emission sites where the overlying air is enriched in methane in the 500 ppm range, including landfills, anaerobic digestor effluents, rice paddy effluents, and oil and gas production sites (12–15). At these sites, methanotrophic methane removal

Significance

Atmospheric methane abundance has risen to a historically high value at 1.92 ppm in 2023 and continues to increase rapidly. A key natural sink for methane is attributed to aerobic methanotrophs that can actively oxidize methane and assimilate the carbon into biomass, and thus, they are candidates for methane removal technology. We demonstrate here that an extant gammaproteobacterial methanotroph, Methylotuvimicrobium buryatense 5GB1C, can grow at low methane concentrations in the range from 200 ppm to 1,000 ppm and exhibits greater methane consumption rates at both low and high methane compared to other methanotroph strains. These features make this strain a promising candidate for methane removal technology at emission sites with enriched methane in air.

Author contributions: L.H., J.D.G., J.F., M.C.K., and M.E.L. designed research; L.H., J.D.G., J.F., and M.C.K. performed research; L.H., J.D.G., E.H.W., J.F., M.C.K., D.A.C.B., and M.E.L. analyzed data; E.H.W. and D.A.C.B. prepared visualizations; and L.H., J.D.G., E.H.W., J.F., M.C.K., D.A.C.B., and M.E.L. wrote the paper.

Reviewers: J.G.F., Pennsylvania State University; and J.D.S., University of Michigan.

The authors declare no competing interest.

Copyright © 2023 the Author(s). Published by PNAS. This open access article is distributed under Creative Commons Attribution-NonCommercial-NoDerivatives License 4.0 (CC BY-NC-ND).

¹Present address: Department of Biological Sciences, California State University Long Beach, Long Beach, CA 90815

²To whom correspondence may be addressed. Email: lidstrom@uw.edu.

This article contains supporting information online at https://www.pnas.org/lookup/suppl/doi:10.1073/pnas. 2310046120/-/DCSupplemental.

Published August 21, 2023.

technology is more likely to be economically feasible at the necessary scale, as demonstrated by studies predicting that sustainable methane removal by methanotrophs is feasible if air contains 500 ppm or more methane (16, 17). A key question then arises regarding which methanotrophs are suitable for such a task, as only a few studies have addressed growth of pure methanotroph cultures fed with methane in the range of 500 ppm (11, 18, 19). We hypothesized that methanotroph strains exist with enhanced abilities to grow on and oxidize methane at 500 ppm.

Results and Discussion

Screening Aerobic Methanotrophs Capable of Growing at 500 ppm Methane. We first carried out a screen for methanotrophs showing strong growth at 500 ppm methane, by testing growth in stoppered serum bottles. Six phylogenetically diverse representatives from both alphaproteobacterial and gammaproteobacterial groups were tested from our culture collection, and of these, M. buryatense 5GB1C, Methylomicrobium (previously Methylosarcina) lacus LW14, Methylosinus sp. LW4, and Methylocystis sp. LW5 were able to grow at 500 ppm methane. However, M. lacus LW14 did not show sustained growth after 10 d at 500 ppm methane. Little or no growth was observed for Methylomonas LW13 or *Methylotuvimicrobium alcaliphilum* 20Z incubated for 14 d (Fig. 1). Additionally, Methylococcus capsulatus (Bath) and Methylosinus trichosporium OB3b, two broadly studied methanotrophs, had previously been shown to not grow or grow poorly at 1,000 ppm or lower concentrations (18), and thus, their growth analyses were not repeated here. In this screen, the four methanotrophs capable of growing at 500 ppm methane show generally linear growth curves (Fig. 1 A, C, D, and F), likely because the headspace in each bottle was refreshed with 500 ppm methane once a day and the daily biomass growth was capped by this restricted supply of methane. Of these four methanotrophs, M. buryatense 5GB1C exhibited the fastest growth and highest optical density values at the end of cultivation at 500 ppm; hence, we focused on this strain in the following analyses. It is worth noting that M. buryatense 5GB1C is also a fast-growing methanotroph at high methane concentrations (25% or 250,000 ppm) with a maximum growth rate of 0.22 h⁻¹ (20).

It is reported that lanthanum (La³⁺) addition in medium, which changes the methanol oxidation system induced, can improve the growth rate of *M. buryatense* 5GB1C by 10% in the presence of sufficient methane (21), but the impact on growth at 500 ppm methane was unknown. We tested the addition of lanthanum, but it did not stimulate growth at 500 ppm methane under the conditions tested (*SI Appendix*, Fig. S1).

Although *M. buryatense* 5GB1C is not predicted to generate N_2O , to confirm the prediction, cultures were tested for N_2O production after growth at 500 ppm methane for 14 d. N_2O concentration in the headspace was measured at 0.22 ± 0.10 ppm, comparable to atmospheric N_2O (0.33 ppm), confirming no N_2O production under these conditions.

Characterization of *M. buryatense* 5GB1C Growth and Kinetic Parameters at Low Methane Concentrations. To more thoroughly evaluate growth performance of *M. buryatense* 5GB1C in response to low methane, we utilized a bioreactor-based system with continuous flow of methane:air mixtures, coupled with gas chromatography (GC) measurement of off-gases. *M. buryatense* 5GB1C was cultivated at seven low methane concentrations (i.e., on 2,500 ppm, 1,000 ppm, 800 ppm, 500 ppm, 300 ppm, 200 ppm, and 100 ppm levels) that were expected to be significantly below the whole-cell K_M for methane $[K_{M(app)}]$, and at 2.5% (v/v, or 25,000 ppm) as a sufficient methane control (Fig. 2 *A* and *B* and *SI Appendix*, Fig. S2 and Table S1). A linear relationship between the methane uptake rate and the specific growth rate was observed for the entire range studied (Fig. 2*B*). These results

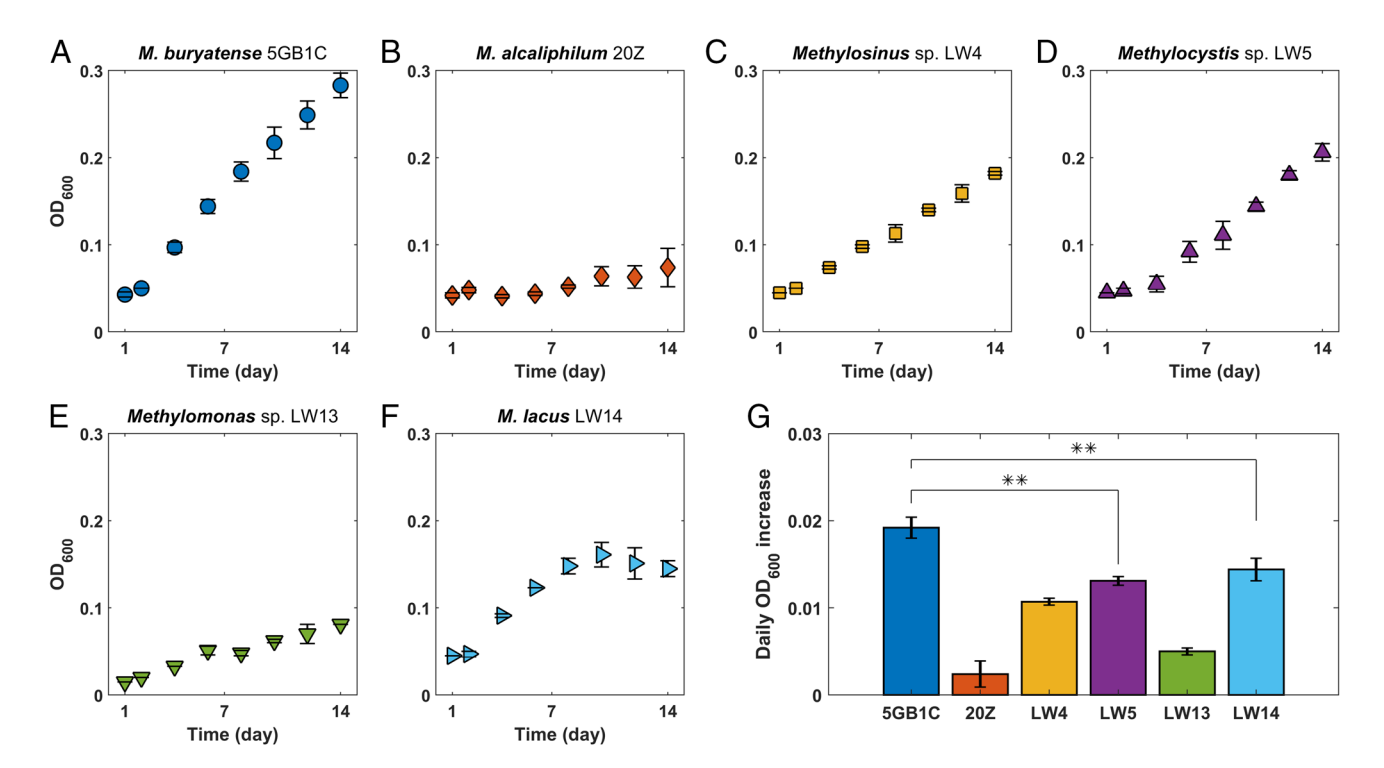


Fig. 1. Growth performance of wild-type methanotrophs at 500 ppm methane. (A-G) Growth curves of M. buryatense 5GB1C (A), M. alcaliphilum 20Z (B), Methylosinus sp. LW4 (C), Methylocystis sp. LW5 (D), Methylomonas sp. LW13 (E), and Methylomicrobium lacus LW14 (E) (D), D0 alphaproteobacteria. (D0 Daily OD600 increase of the seven methanotrophs during a 14-d growth period (D1 sy which were determined based on the slopes of the linear region of growth curves. **P1 C 0.01, which was determined by the unpaired D1 test. Error bars represent SDs.

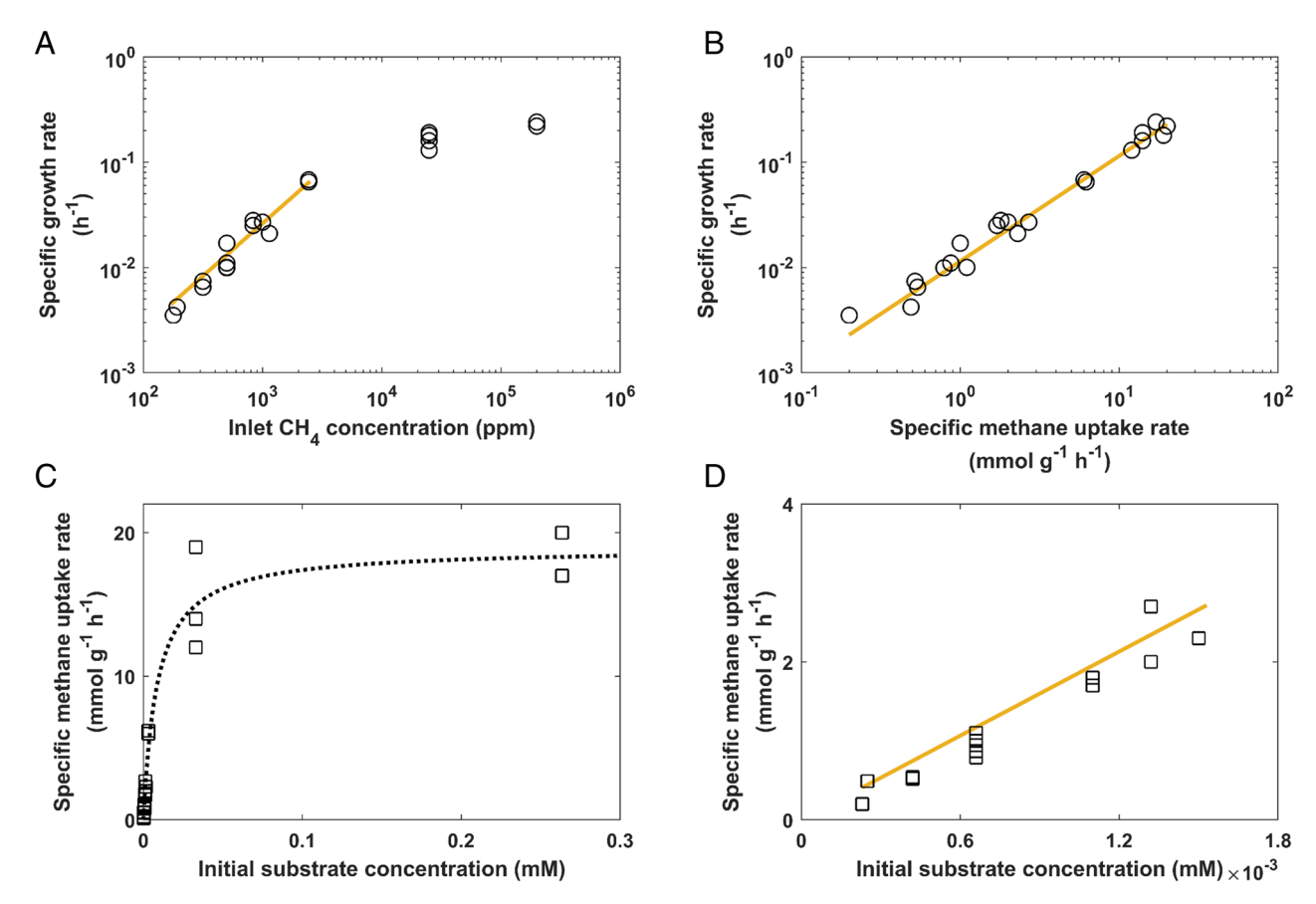


Fig. 2. Characterization of growth and kinetic parameters of *M. buryatense* 5GB1C. (*A*) Relationship between specific growth rates and the methane concentrations of inlet gas. In the range between 200 ppm and 2,500 ppm methane, the yellow line represents the fitted linear regression curve ($R^2 = 0.82$, $P = 1.2 \times 10^{-5}$). Growth data at 20% (v/v) or 200,000 ppm CH₄ balanced with 5% O₂ and 75% N₂ were based on a previous report (22). (*B*) A linear relationship between the specific growth rate and the methane uptake rate. The yellow line represents the fitted linear regression curve ($R^2 = 0.96$, $P = 3.6 \times 10^{-15}$). (*C*) The Michaelis–Menten plot of whole-cell methane uptake rate [mmol methane (gram cell dry weight)⁻¹ h⁻¹] as a function of initial substrate concentration was calculated based on Henry's law (*Methods and Materials*). (*D*) Linear regression of the linear region of the Michaelis–Menten curve ($R^2 = 0.93$, $P = 6.6 \times 10^{-8}$). Each symbol represents an independent measurement.

also show that M. buryatense 5GB1C is able to grow below 500 ppm methane, with growth observed as low as ~200 ppm methane (Fig. 2 A and B and SI Appendix, Tables S1 and S2). No other gammaproteobacterial methanotrophs have been shown to grow at such low methane concentrations (11, 18, 19). At ~100 ppm methane, we observed initial growth of M. buryatense 5GB1C for 2 wk; however, biomass barely increased afterward (SI Appendix, Fig. S2C). The culture was allowed to recover for 17 h at ~600 ppm methane and then switched to ~100 ppm methane, but the same behavior was observed (SI Appendix, Fig. S2C). These results indicate that 100 ppm methane may not support long-term growth of M. buryatense 5GB1C. Notably, some alphaproteobacterial methanotrophs have been shown to grow at 100 ppm and lower methane, including Methylocystis species (18, 19) and *Methylocapsa gorgona* MG08 (11). However, two Methylocystis strains for which data are available grew two to threefold more slowly than M. buryatense 5GB1C at 1,000 ppm methane and M. gorgona MG08 showed sixfold lower methane oxidation rates at 800 ppm methane (SI Appendix, Tables S1 and S2). Assuming a similar linear relationship for the methanotrophs listed in SI Appendix, Table S2, it may be predicted that they would also grow more slowly and consume methane at lower rates than M. buryatense 5GB1C at 200 to 500 ppm methane. Finally, our measurements reveal a strong linear correlation for M. buryatense 5GB1C between the specific growth rate and the methane concentration of the inlet gas from

200 ppm to 2,500 ppm, corresponding to specific growth rates from 0.004 to 0.07 h⁻¹ (Fig. 2A).

In methanotrophs, a part of the energy produced from methane oxidation is allocated for cell maintenance. For M. buryatense 5GB1C grown at methane sufficiency (14% methane; 140,000 ppm), the non-growth-associated ATP maintenance energy (NG-ATPM) is 10 to 15 mmol ATP per gram of dry weight per hour (mmol ATP $g^{-1} h^{-1}$) (23). However, *M. buryatense* 5GB1C grown with 200 ppm methane exhibits a methane uptake rate of 0.2 to 0.5 mmol methane g⁻¹ h⁻¹ (Fig. 2 A and B and SI Appendix, Table S1) and thus can only yield up to 3.0 mmol ATP g⁻¹ h⁻¹ assuming six mole ATP generated per mole of methane consumed (24). Since during active growth, the methane consumed must be partitioned into carbon allocated for biomass generation and carbon for ATP generation, the actual NG-ATPM must be significantly lower than 3.0 mmol ATP g⁻¹ h⁻¹. Indeed, fitting our measurements with the Herbert-Pirt model (25) yielded an NG-ATPM of 0.36 mmol ATP g⁻¹ h⁻¹ (*SI Appendix*, Fig. S3A), comparable to the NG-ATPM (0.6 mmol ATP g⁻¹ h⁻¹) required for retentostat-grown Saccharomyces cerevisiae at a growth rate of ~0.001 h⁻¹ (26). However, the NG-ATPM derived from the linear regression has a high P value (0.75) and a wide 95% CI from 0 to 2.8 mmol ATP g⁻¹ h⁻¹ (SI Appendix, Fig. S3A). We also used a genome-scale reconstruction (GEM) model (27) to predict growth rates at 1,000 ppm methane or lower. Results show that the NG-ATPM must be ~0.4 mmol ATP g⁻¹ h⁻¹ or lower to allow

reasonable growth rate predictions at low methane concentrations (SI Appendix, Fig. S3 B-D). These findings suggest that M. buryatense 5GB1C is able to decrease the NG-ATPM as a function of decreased substrate availability, as reported previously for *S. cere*visiae (26). It may be predicted that such a capability could contribute to the relatively strong growth of M. buryatense 5GB1C at low methane, since it would enhance the energy from methane oxidation available to support biomass production.

It has been suggested that methanotrophs able to grow at 100 ppm methane and below contain a special high-affinity pMMO (18, 19), although this is apparently not the case in M. gorgona MG08 (11). To assess whether M. buryatense 5GB1C might show methane oxidation kinetics indicative of a high-affinity pMMO, we carried out whole-cell Michaelis-Menten analysis (Fig. 2C), determining that the whole-cell $K_{\rm m}$ [$K_{\rm M(app)}$] and the whole-cell V_{max} ($V_{max(app)}$) for methane are 8.8 ± 1.7 μM (equivalent to 6,681 ± 1,291 ppm methane in the gas phase at equilibrium) and 18.9 ± 0.9 mmol g⁻¹ h⁻¹, respectively. Although the $V_{max(app)}$ is higher than other known methanotrophs, indicating a rapid maximum methane oxidation rate, $K_{M(app)}$ is also high compared to other methanotrophs (18). This result does not support the idea that M. buryatense 5GB1C possesses a pMMO with higher affinity to methane than other known methanotrophs. It has been well established that $K_{M(app)}$ is in part dependent on the overall expression of pMMO (18). The specific affinity as which denotes the slope of the linear part of the Michaelis-Menten curve, has been suggested to be a more suitable parameter for comparing methane oxidation rates among methanotrophs at low concentrations (18, 19). Through a linear regression (Fig. 2D), as of for *M. buryatense* 5GB1C is determined to be $1{,}101 \pm 87 \times 10^{-12}$ L cell⁻¹ h^{-1} (or 1,776 ± 140 L g^{-1} h^{-1}), more than fivefold larger than the highest reported value and 30 to 100-fold higher than most tested methanotrophs (11, 18, 19) (SI Appendix, Table S2), in keeping with the ability of this methanotroph to grow at methane significantly below the $K_{M(app)}$. The underlying mechanism for high as is unknown. pMMO phylogenetic analysis suggests that the high as measured for M. buryatense 5GB1C is likely not due to a high-affinity pMMO, since the M. buryatense 5GB1C pMMO subunit DNA sequences are closely related to other gammaproteobacterial pMMO sequences, including those of methanotrophs unable to grow at 500 ppm methane (28).

At low growth rates, bacteria may display significant morphological changes (25). We thus quantified biomass dry weight per OD₆₀₀ unit, cell sizes, and the coverage of intracytoplasmic membranes (ICMs) that house pMMO. No significant changes were found in any of these parameters between low (500 ppm methane or less) and high (2.5% or more) methane growth conditions (SI Appendix, Fig. S4), which indicates robustness of cell morphology. Particularly, we found a moderate 20% reduction of ICM coverage in cells at 500 ppm methane but without statistical significance (SI Appendix, Fig. S4A).

Transcriptional Response of M. buryatense 5GB1C to Low **Methane.** In some bacteria, strong transcriptional responses accompany growth under nutrient limitation and at low growth rates: Bacteria often decrease expression of the translation and transcription apparatus, up-regulate functions involved in motility and chemotaxis, and up-regulate amino acid synthesis pathways (25, 29–31). To understand how *M. buryatense* 5GB1C responds to low methane at the transcriptional level, we quantified holistic gene expression of cultures grown at 500 ppm and 1,000 ppm at methane-limited steady-state in the bioreactor, with growth rates of 0.009 h⁻¹ and 0.02 h⁻¹, respectively. Differentially expressed genes are defined as those exhibiting an absolute log₂-fold change

over one and adjusted p value less than 0.05 in comparison to a reference condition, i.e., methane-limited steady-state growth on 2.5% (v/v) methane at a growth rate of $\sim 0.125 \text{ h}^{-1}$ (22).

Transcription profiles of M. buryatense 5GB1C at 500 ppm and 1,000 ppm methane are highly consistent with each other, without any significant variations in gene expression (SI Appendix, Fig. S5). When compared to transcriptional profiles under 2.5% methane conditions (32), 725 genes are differentially expressed at both 500 ppm and 1,000 ppm methane (Fig. 3A and Dataset S1). Of note, two cold-shock proteins, which are RNA chaperones and in other bacteria are involved in regulation of transcription and translation under stress (33), show strongly changed gene expression but with divergent trends: One (EQU24_ RS15705) is down-regulated by two log₂-fold, while the other (EQU24_RS16055) is up-regulated by over three log₂-fold. Transposases are highly up-regulated in general; however, many but not all of their gene expression levels are low in transcripts per million (TPM < 10) (Dataset S1). Cells under stress commonly up-regulate transposase expression (34).

We also analyzed expression of specific genes involved in central metabolism. In the pathway converting methane to CO₂, genes encoding pMMO (converts methane to methanol) and the MxaF-type methanol dehydrogenase (converts methanol to formaldehyde) are highly expressed but with no significant variations (Fig. 3B). Transcriptional levels of the tetrahydromethanopterin (H₄MPT) pathway (converts formaldehyde to formate) remain unperturbed except for two genes encoding formaldehyde-activating enzyme (EQU24_RS13345 and EQU24_RS14315) displaying significant variations in expression. All six genes encoding two formate dehydrogenases (convert formate to CO₂) are down-regulated, with greater decreases at 500 ppm methane than at 1,000 ppm methane. These results are accordant with the observation that the excreted formate rate is roughly two times higher at 500 ppm methane (0.018 \pm 0.002 mmol formate g $^{-1}$ h $^{-1}$) than at 1,000 ppm methane $(0.009 \pm 0.003 \text{ mmol formate g}^{-1} \text{ h}^{-1})$. These values are much lower than corresponding methane uptake rates (0.95 ± 0.08) mmol CH₄ g^{-1} h^{-1} at 500 ppm and 1.5 ± 0.2 mmol CH₄ g^{-1} h^{-1} at 1,000 ppm, SI Appendix, Table S1), suggesting that cells growing at low methane tend to reduce carbon loss as formate or CO₂ to allow more carbon assimilation. Gene expression of other central metabolic pathways remains mostly unchanged (Fig. 3B), including glycolysis, the tricarboxylic acid cycle, and the ribulose monophosphate cycle (converts formaldehyde and ribulose 5-phosphate to three-carbon compounds for assimilation). One exception is the incomplete serine cycle (converts formate and CO₂ to acetyl-CoA), where the malate-CoA ligase (EQU24_ RS04635) and the malyl-CoA lyase (EQU24_RS04630) are down-regulated by two log₂-fold. Taken together, these results suggest that although the growth rate is decreased by over an order of magnitude, expression of the proteins important for central metabolism pathways is largely unchanged. Such a response is in keeping with a strategy to poise the cells to take advantage of whatever methane is available under these strongly methane-limiting growth conditions.

As for energy metabolism, the NADH-ubiquinone reductase and the F₁F₀-type ATP synthase are strongly down-regulated, in keeping with the greatly decreased energy needs at these low growth rates (Fig. 3C).

Gene expression for biosynthesis pathways of fatty acids, amino acids, nucleotides, vitamins, and cofactors remain either stable or down-regulated (Fig. 3D), again, in keeping with the low growth rates and expected decreased fluxes through these pathways. In contrast, genes glgA (EQU24_RS18670) and glgB (EQU24_ RS18665) associated with glycogen synthesis are up-regulated by

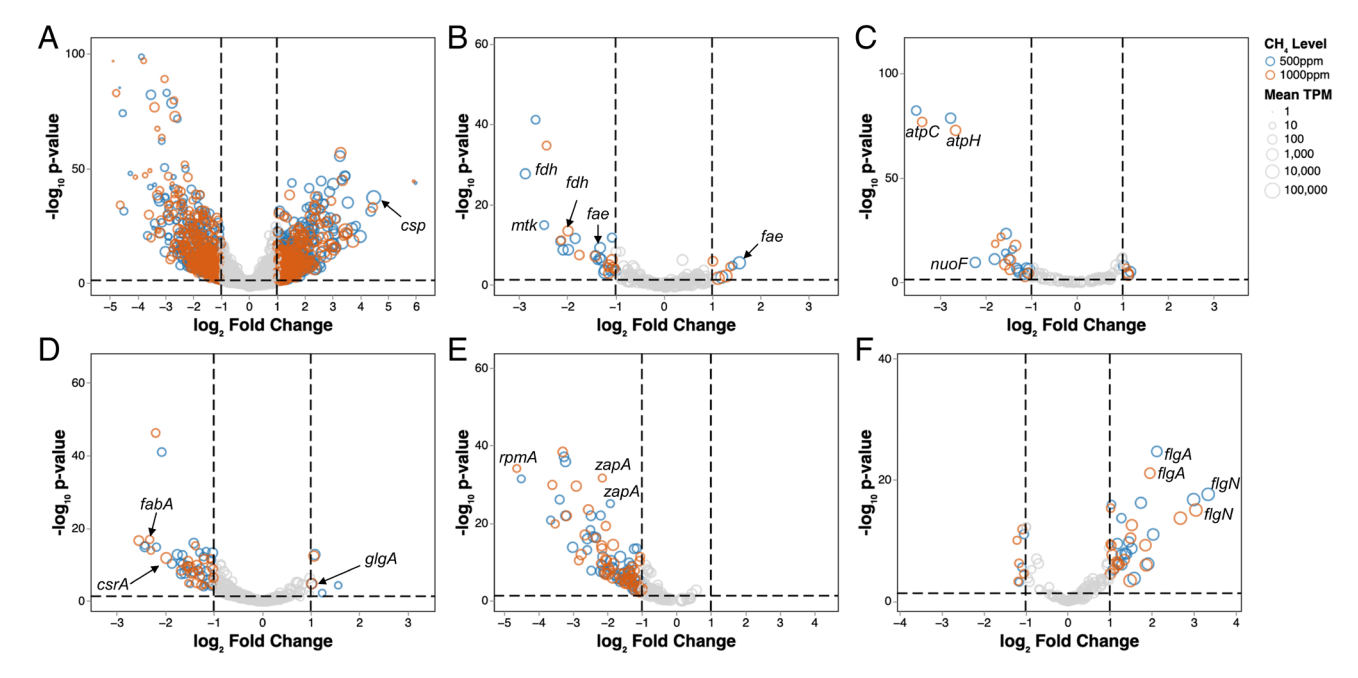


Fig. 3. Transcriptional changes of *M. buryatense* 5GB1C grown at 500 ppm (blue) and 1,000 ppm (orange) methane in comparison to 2.5% (v/v) methane growth conditions. (*A-F*) Volcano plots of gene expression changes of the entire genome (*A*), core central carbon metabolism (*B*), energy metabolism (*C*), biosynthesis of building blocks and cofactors (*D*), translation and transcription apparatus (*E*), and motility and chemotaxis (*F*). Symbol sizes are correlated with gene expression as shown in the figure. The horizontal dashed line represents P = 0.05. The two vertical dashed lines represent \log_2 -fold at -1 and 1, respectively. Genes that do not change significantly are colored in gray. Gene abbreviations and gene products: *csp*, cold shock protein; *fae*, formaldehyde activating enzyme; *fdh*, formate dehydrogenase; *mtk*, malate-CoA ligase; *atpC*, F_1F_0 type ATP synthase subunit epsilon; *atpH*, F_1F_0 type ATP synthase subunit builting enzyme; *fabA*, 3-hydroxyacyl-[acyl-carrier-protein] dehydratase FabA; *csrA*, carbon storage regulator CsrA; *glyA*, glycogen synthase GlgA; *zapA*, cell division protein ZapA; *rpmA*, 50S ribosomal protein L27; *flgA*, flagellar basal body P-ring formation chaperone FlgA; *flgN*, flagellar protein FlgN. An interactive version of this figure is available at https://erinhwilson.github.io/limited-ch4-tpm-analysis/.

about one log₂-fold, while other related genes including those for glycogen degradation do not show significant changes in expression. This is consistent with downregulation (1.5 to 2.0 log₂-fold) of the carbon storage regulator *csrA* (EQU24_RS07950), which has been shown to negatively mediate glycogen synthesis in *Escherichia coli* (35). It is not clear why the cells would increase carbon storage, but it may reflect a strategy to prepare the cells to accommodate future starvation.

We also observed a strong decline in gene expression of ribosomal proteins, tRNA-ligases, RNA polymerases, and sigma factors (Fig. 3E), suggesting a slowdown of transcription and translation processes. Cell division genes, such as ftsL (EQU24_RS19745), ftsB (EQU24_RS13310), and zapA (EQU24_RS04165), are also significantly down-regulated (Fig. 3E). These changes also reflect decreased need at the low growth rates. By contrast, many genes related to flagellar protein synthesis and chemotaxis are up-regulated (Fig. 3F), as bacteria tend to be more active in searching for nutrients and more favorable environments under stress (29).

All in all, the transcriptional response is in keeping with the low NG-ATPM values, in which the cells down-regulate functions that are not needed at low growth rates, while maintaining or up-regulating those functions that will poise the cells to take advantage of better growth conditions, or alternatively, the onset of complete carbon starvation.

Global Removal Projections. In order to assess whether this improved performance of methane removal at 500 ppm could theoretically be feasible for a future methane removal technology, we have carried out projections based on our results compared to literature results. Many examples exist of methanotroph-based biofilter technology for removing methane from waste streams, but the majority of these are carried out at 10,000 ppm (1%) methane

or higher and involve "wild" mixed methanotroph communities (consortia), enriched with high (greater than 1%) methane (36). In the few cases in which methane inlet concentrations below 1% have been reported, elimination capacities (ECs) at 500 ppm methane are estimated to be in the range of 0.5 to 3.2 g CH₄ removed $m^{-3} h^{-1} (37-39)$ (SI Appendix, Table S3). With the 121 m³ treatment unit size used in a previous modeling study (16) and assuming 7,200 h (300 d) (16) operation per year, such ECs are projected to result in removal of 0.4 to 2.8 tons methane per year per treatment unit at 500 ppm methane. At the higher end, these ECs are similar to the 5 tons methane per year predicted for pure cultures of methanotrophs (16), strains that are known to not grow significantly at 500 ppm methane (18). These results suggest that the methanotroph strains enriched in published biofilter experiments may not be well-suited for removing such low methane. We have shown the M. buryatense 5GB1C specific affinity is more than fivefold higher than the highest reported values and 30 to 100-fold higher than most methanotrophs enriched at high methane. Thus, in theory, the EC for 500 ppm methane with M. buryatense 5GB1C should be at least fivefold greater than those in the literature, increasing to 2 to 14 ton per year per treatment unit, and could be significantly higher. The actual EC would depend on how well this strain performs under such conditions compared to general methanotrophs.

Given known biomass yields for *M. buryatense* 5GB1C (22), 0.78 ton biomass dry weight is predicted to be formed per ton methane utilized (*Methods and Materials*). Methane-derived biomass (single cell protein) has been used for aquaculture feed and is predicted to have a value of ~\$1,600 per ton (40), a cobenefit of methane removal by methanotrophs. If bioreactor systems could be developed that would allow automated biomass harvesting, this cobenefit could substantially add to the attractiveness of a bio-based methane removal system.

Standard biofilters are not designed for use of low methane and alternative bioreactor configurations that focus on enhanced mass transfer could significantly increase ECs at these low methane inlet concentrations. If a combination of strain improvement and bioreactor/bioprocess design could increase ECs 20-fold, treatment units would be projected to remove 40 to 280 tons methane per year. In such a case, 50,000 to 300,000 units deployed worldwide for 20 y at sites with methane enrichment in air averaging 500 ppm would keep 240 million tons methane from entering the atmosphere, an outcome predicted to significantly impact global warming (1, 5). A previous economic analysis (16) suggests that a 20-fold improvement in EC would also become economically feasible, but full environmental life cycle and technoeconomic analyses are needed to more definitively address economic and environmental impacts. The above analysis suggests the use M. buryatense 5GB1C either by itself or as part of a consortium as the basis of a methane treatment technology is potentially feasible in the 500 ppm range. More studies are necessary to determine actual feasibility under field conditions.

In summary, M. buryatense 5GB1C has emerged from our screening study as a promising candidate for a methane removal technology that does not increase N₂O emissions, and our results suggest that its ability to grow at low methane relies at least partly on a high specific affinity and a low maintenance energy. The former denotes an inherently rapid methane assimilation that provides the basis for energy production and biomass growth. The latter is in keeping with drastic downregulation of translation and transcription machineries, as both synthesis and maintenance of those components are energy-demanding. They both confer growth advantages in the face of severe substrate limitation, enhancing the energy produced from methane oxidation that can be invested into biomass synthesis. This well-studied bacterium is an excellent candidate to serve as a platform for developing methane removal technology either by itself or as part of a consortium. Strain improvements could be carried out using approaches such as adaptive laboratory evolution and targeted genetic manipulations to improve growth at low methane, and growth improvements could involve testing other medium constituents such as copper concentration. Moving forward, research should also be focused on integration of these methane consumers into deployable and scalable bioreactor systems as well as environmental life cycle and technoeconomic analyses of such a methane removal technology to ensure both economic feasibility and environmental benefit.

Methods and Materials

Strains and Bacterial Cultivation. Methylosinus sp. LW4, Methylocystis sp. LW5, Methylomonas sp. LW13, and Methylomicrobium (formerly Methylosarcina) lacus LW14 (41) were grown in nitrate mineral salts (NMS) medium (42). Methylotuvimicrobium buryatense 5GB1C and Methylotuvimicrobium alcaliphilum 20Z^R were grown in NMS2 medium (20). All methanotrophs were cultivated at 30 °C throughout this study.

To test methanotrophic growth at low methane, colonies of methanotrophs were inoculated into 5 mL fresh medium in glass tubes (18-by-150 mm with an interior volume of ~27.5 mL) sealed with stoppers (20 mm in diameter). Precultures were first grown with 20% (v/v) methane in the headspace and shaken at 200 rpm and then subcultured in 10 mL fresh medium with an initial optical density at 600 nm (OD $_{600}$) between 0.02 and 0.05 in serum bottles (with an interior volume of ~250 mL). Next, 5 mL of certified 2.5% (v/v) methane:air gas (Linde plc) was injected into stoppered bottles, yielding approximately 500 ppm methane in the headspace. The headspace was refreshed daily with the corresponding methane:air gas mixtures. Also, 0.2 mL to 0.3 mL samples were taken and diluted three to five times with sterile media for OD₆₀₀ measurements using a Jenway® 7300 Spectrophotometer. Similar experiments were also carried out with glass tubes. Briefly, precultures were subcultured in fresh medium with an

OD₆₀₀ between 0.01 and 0.03. Next, 0.5 mL, 1 mL, or 5 mL of certified 2.5% (v/v) methane:air gas (Linde plc) was injected into the stoppered glass tubes, yielding approximately 500 ppm, 1,000 ppm, or 5,000 ppm methane in the headspace, respectively. OD₆₀₀ values were measured by a spectrophotometer (Thermo Scientific™ Spectronic™ 20D+). The daily OD₆₀₀ increase was determined by the slope of growth curves in the linear region. N₂O concentration in the headspace was measured after 14 d of growth by a gas chromatograph (GC) (Model 8610, SRI Instrument) equipped with an electron capture detector as previously described (43). During La³⁺ addition experiments, glass tubes were acid-washed with 1M HCl overnight and then rinsed with ddH₂O before use.

Bioreactor Setup and Gas Chromatography Measurements. The bioreactor was operated as described (22, 44). Briefly, M. buryatense 5GB1C growing at the middle to late exponential growth phase was inoculated into 1 LNMS2 medium in the bioreactor (New Brunswick Scientific) connected to the BioFlo® &Celligen® 310 control system (New Brunswick Scientific). Per liter of NMS2 medium, 10 mL 1M carbonate buffer was added. The culture was agitated constantly at 1,000 rpm, and the temperature was maintained at 30 °C. Inlet gas was filtered by a 0.2 µm autoclavable membrane (Whatman plc), and the flow rate was controlled by a mass flow controller (SmartTrak®100, Sierra). The off-gas was automatically sampled every 15 min by a GC (Model GC-2014, Shimadzu Corporation, Japan) equipped with a thermal conductivity detector, as described (31). OD_{600} values were measured using a Jenway® 7300 Spectrophotometer.

An empirical calibration curve for methane was obtained by using certified standard methane:air gas mixtures, i.e., 500 ppm, 1,000 ppm, and 2.5% (v/v) methane:air gases. The equation was: y = 0.0049x + 0.0003 ($R^2 > 0.99$), where y is the methane concentration (%), and x is the peak area (μV·min) divided by 100. All standard gas tanks were purchased from Linde plc.

In batch conditions, 2.5% methane:air gas was diluted with air at different ratios to create gas mixtures of different methane concentrations. The flow rate of air was constant at 100 cm³ min⁻¹, while the flow rate of 2.5% methane:air gas was set to different rates. Methane concentrations of the resulting mixtures were measured by GC with the calibration curve, and these varied somewhat between experiments (SI Appendix, Table S1).

For steady-state (chemostat) conditions, certified 500 ppm or 1,000 ppm methane:air gas was delivered to M. buryatense 5GB1C at a flow rate of 100 cm³ min⁻¹, which underwent a sequence of growth stages: batch growth at 1,000 ppm methane, chemostat (steady-state) growth at 1,000 ppm methane (0.02 h^{-1}) , chemostat (steady-state) growth at 500 ppm methane (0.009 h^{-1}) , and batch growth at 500 ppm methane (SI Appendix, Fig. S3). To quantify formate production, 0.8 mL culture was collected from chemostat-grown cultures and pelleted at room temperature. The supernatant was filtered in SpinX® centrifuge tubes (Corning® Costar®) equipped with 0.2 µm membranes at 10,000 ×g for 1 min and stored at -20 °C. Formate concentrations were determined by an ion chromatography system (ICS-5000 ion, Thermo Fisher Scientific) equipped with a Dionex IonPac ICE-AS6 column (9 by 250 mm, Thermo Fisher Scientific) as previously described (27).

RNA Isolation and RNAseq Analysis. After growth of three generations under steady-state conditions, ~80 mL culture was harvested in Falcon™ tubes precooled with liquid N_2 , and then, samples were centrifuged at 6,000 \times g for 15 min at 4 °C. The remainder of the procedures for RNA isolation were the same as described previously (21). RNA samples were stored at -80 °C before submission to Azenta/GENEWIZ (USA) for sequencing.

Standard bioinformatics tools were used to process the RNASeq data, assisted by the barrelseq workflow, which is available on Github: https://github.com/ BeckResearchLab/barrelseq (DOI: 10.5281/zenodo.4323588). Briefly, reads from the fastg field were aligned to the M. buryatense 5GB1C genome (NCBI accession NZ_CP035467.1) using BWA with the BWA-MEM algorithm (BWA version 0.7.17-r1198-dirty, default parameters) (45). SAMTools version 1.9 was used to transform the initial read alignments into sorted BAM files (46). The htseq-count tool from the "HTSeq" framework version 2.0.2 was used with modifications (described below) to attribute the reads to ORFs using the "intersectionnonempty" mode, providing estimates of raw read counts (47). Statistical evaluation for differential expression was performed using DeSeq2_1.2.10 on the raw read counts. Raw read counts were subsequently converted into TPM for each genome feature for use in visualizations (48).

htseq-count was modified to enable the counting of multiply-mapped reads. By default, multiply-mapped reads are assigned an alignment quality of 0 and ignored during counting. In the context of M. buryatense, several key genes (phi, hps, and tkt, encoding 6-phospho-3-hexuloisomerase, 3-hexulose-6-phosphate synthase, and transketolase, respectively) in the RuMP pathway occur in a cluster of 4 tandem repeats (EQU24_RS22575 - EQU24_RS21610, EQU24_RS23130-EQU24_RS23165), resulting in most reads for these genes mapping equally well to multiple locations and thus being ignored. In order to include these genes in our expression analyses, htseq-count was modified to process these reads by distributing their counts across the locations where they mapped with equal quality. The modified htseq-count code to support this mode of counting is available here: 10.5281/zenodo.7434230).

Measurements of Growth and Kinetic Parameters. The overall methane consumption rate of the entire culture $(q, \text{in mmol h}^{-1})$ at concentrations lower than 2,500 ppm methane was determined by the following equation: $q = \frac{P_i - P_o}{R \cdot T} \cdot Q$, where P_i and P_o are partial pressures of methane in the inlet gas and off-gas, respectively; R is the ideal gas constant; T is the temperature; and Q is the inlet gas flow rate. When the methane concentration was 2.5% (v/v) or above, q was determined as previously described (44).

In batch conditions, the specific methane uptake rate (V, in mmol g^{-1} h^{-1}) was determined by the slope of the overall methane consumption rate (q) against the total biomass dry weight (TDW), i.e., $V = \frac{dq}{dTDW}$. The specific growth rate (μ) was determined by the slope of natural log values of TDW against time, i.e., $\mu = \frac{d \ln (TDW)}{dt}$. At least three data points in the exponential growth phase were used for calculating the above parameters. The conversion between the optical density and biomass dry weight was based on previous measurements (22) and reconfirmed in this study for growth at 200 ppm methane. Sample volumes were recorded to correct the culture volume in the bioreactor.

In chemostat conditions, $V=\frac{q}{TDW^i}$ and the specific growth rate (μ) was equal to the dilution rate (D): $\mu=D=\frac{Vol_{out}}{Vol_{5G}}$, where Vol_{out} is the volume of culture pumped out of the bioreactor per unit time and Vol_{5G} is the total M. buryatense 5GB1C culture volume (\sim 1 L).

The whole-cell K_M [$K_{M(app)}$] and the whole-cell maximum methane uptake rate (V_{max}) were determined via fitting experimental data with the equation $V = V_{max(app)} \frac{S}{K_{M(app)} + S}$, where S is the initial substrate concentration in the liquid phase. Nonlinear regression and statistics were performed by the built-in function "fitnlm" in MATLAB (Version 2022b). S was calculated as follows: $S = H \cdot P_{CH4}$, where H is the Henry's constant for methane at 30 °C (1.3 \times 10⁻⁵ mol m⁻³ Pa⁻¹) (49), and P_{CH4} is the partial pressure of methane. The specific affinity ao_s was calculated by the slope of the linear section of the Michaelis–Menten curve: $a_s^o = \frac{dV}{dS}$. Linear regression and statistics were performed by using "fitlm" in

Flux Balance Analysis. The GEM model of *M. buryatense* 5GB1C was based on a previous study (27). Given different specific methane uptake rates, the GEM

model was used to predict corresponding growth rates with varied NG-ATPM values. Simulation was carried out in both COBRAPy (50) and MATLAB.

Measurement of Intracytoplasmic Membrane Coverage, Cell Size, and Dry Weight. *M. buryatense* 5GB1C cells grown at 2.5% and 500 ppm methane were harvested at $6,000 \times g$ for 10 min at room temperature, and washed with 1 mL of 1× phosphate-buffered saline, pH 7.4 (PBS, Invitrogen). Of note, 1 to 5 mL of cells in the exponential phase were harvested to achieve a final OD₆₀₀ of 1.0 when resuspended in 1 mL of PBS. Cells were pelleted at $6,000 \times g$ for 10 min and resuspended in 1 mL 4% paraformaldehyde (w/v) (Sigma-Aldrich) in PBS. The cells were incubated on ice for 30 min and then pelleted and washed twice with PBS. The final cell suspensions were stored at 4 °C until staining.

Cells were stained with FM 1-43 (ThermoFisher/Invitrogen, Waltham, MA, USA) to a final concentration of 5 μg mL $^{-1}$ in PBS for 1 h at 25 °C. Then cells were placed on a glass slide coated with 0.01% poly-l-lysine (Sigma-Aldrich, St. Louis, MO, USA), topped with a coverslip, and sealed. All images were captured on a Nikon C2si confocal microscope with a 60 × Plan Apo λ (NA 1.45) oil objective using a pinhole radius at 0.3 μm . The fluorophore excitation wavelength was 488 nm with emission detected with a spectral filter of 490 to 560 nm. All the imaging was performed at room temperature, immediately after staining. Individual cell images were analyzed using NIS-Elements AR Analysis 4.30.02 software (Nikon) to calculate the percent ICM by comparing the total area of the cell (cell size) to the area of internal fluorescence, as previously described (51).

Cell dry weights were measured as described previously (22). Briefly, 225 mL cultures were harvested and centrifuged at 6,000 \times g for 75 min in preweighed tubes. After the supernatant was removed, samples were washed with sterile ddH $_2$ O and centrifuged at 6,000 \times g for 30 min. The supernatant was discarded, and cell pellets were lyophilized overnight (Labconco® FreeZone® 4.5 L $-105\,^{\circ}$ C Benchtop Freeze Dryer) before weight measurements.

Calculation of Biomass Efficiency. *M. buryatense* 5GB1C yields (g C in biomass/g C in CH_4) average 0.5 (22). Assuming the cells are 48% C dry weight (52) and converting to ton CH_4 , each ton of CH_4 would generate 0.78 ton biomass.

Data, Materials, and Software Availability. The RNA-Seq data have been uploaded to the NCBI Gene Expression Omnibus (GEO) under accession number GSE221011 (53). An interactive version of Fig. 3 is available at https://erinhwilson.github.io/limited-ch4-tpm-analysis/.

ACKNOWLEDGMENTS. We thank Britt Abrahamson and Dr. Kristopher A. Hunt for their assistance on the formate and N_2O measurements. The work at University of Washington was supported by NSF awards MCB-2223496 and CBET-2218298 and by the Jungers Endowed Chair. Work at the United States Naval Academy was supported by the John F. Kelley Biosciences Fund.

Author affiliations: ^aDepartment of Chemical Engineering, University of Washington, Seattle, WA 98195; ^bSchool of Computer Science & Engineering, University of Washington, Seattle, WA 98195; ^cDepartment of Chemistry, US Naval Academy, Annapolis, MD 21402; ^ceScience Institute, University of Washington, Seattle, WA 98195; and ^cDepartment of Microbiology, University of Washington, Seattle, WA 98195

- S. Abernethy, F. M. O'Connor, C. D. Jones, R. B. Jackson, Methane removal and the proportional reductions in surface temperature and ozone. *Philos. Trans. R. Soc. A Math. Phys. Eng. Sci.* 379, 20210104 (2021).
- IPCC et al., IPCC, 2021: Climate Change 2021: The Physical Science Basis (Cambridge University Press, 2021).
- E. J. Dlugokencky, NOAA/GML (2022). https://gml.noaa.gov/ccgg/trends_ch4/.
- . M. Saunois et al., The global methane budget 2000–2017. Earth Syst. Sci. Data 12, 1561–1623 (2020)
- I. B. Ocko et al., Acting rapidly to deploy readily available methane mitigation measures by sector can immediately slow global warming. Environ. Res. Lett. 16, 054042 (2021).
- P. B. R. Nisbet-Jones et al., Is the destruction or removal of atmospheric methane a worthwhile option? Philos. Trans. R. Soc. A Math. Phys. Eng. Sci. 380, 20210108 (2022).
- L. Warszawski et al., All options, not silver bullets, needed to limit global warming to 1.5 °C: A scenario appraisal. Environ. Res. Lett. 16, 064037 (2021).
- R. B. Jackson et al., Atmospheric methane removal: A research agenda. Philos. Trans. R. Soc. A Math. Phys. Eng. Sci. 379, 20200454 (2021).
- Sci. 379, 20200454 (2021).
 T. Sun, I. B. Ocko, E. Sturcken, S. P. Hamburg, Path to net zero is critical to climate outcome. Sci. Rep.
- J. Chang et al., Methanobactin from Methylosinus trichosporium OB3b inhibits N₂O reduction in denitrifiers. ISME J. 12, 2086–2089 (2018).

- A. T. Tveit et al., Widespread soil bacterium that oxidizes atmospheric methane. Proc. Natl. Acad. Sci. U.S.A. 116, 8515–8524 (2019).
- G. Börjesson et al., A national landfill methane budget for Sweden based on field measurements, and an evaluation of IPCC models. Tellus, Ser. B Chem. Phys. Meteorol. 61 B, 424–435 (2009).
- I. Irakulis-Loitxate et al., Satellite-based survey of extreme methane emissions in the Permian basin. Sci. Adv. 7, eabf4507 (2021).
- M. J. Bell et al., Variation in enteric methane emissions among cows on commercial dairy farms. Animal 8, 1540–1546 (2014).
- M. R. J. Daelman, E. M. van Voorthuizen, U. G. J. M. van Dongen, E. I. P. Volcke, M. C. M. van Loosdrecht, Methane emission during municipal wastewater treatment. Water Res. 46, 3657–3670 (2012).
- S. Yoon, J. N. Carey, J. D. Semrau, Feasibility of atmospheric methane removal using methanotrophic biotrickling filters. Appl. Microbiol. Biotechnol. 83, 949-956 (2009).
- Y. Cai, Y. Zheng, P. L. E. Bodelier, R. Conrad, Z. Jia, Conventional methanotrophs are responsible for atmospheric methane oxidation in paddy soils. *Nat. Commun.* 7, 1–10 (2016).
- C. Knief, P. F. Dunfield, Response and adaptation of different methanotrophic bacteria to low methane mixing ratios. *Environ. Microbiol.* 7, 1307–1317 (2005).
- M. Baani, W. Liesack, Two isozymes of particulate methane monooxygenase with different methane oxidation kinetics are found in *Methylocystis* sp. strain SC2. *Proc. Natl. Acad. Sci. U.S.A.* 105, 10203–10208 (2008).

- A. W. Puri et al., Genetic tools for the industrially promising methanotroph Methylomicrobium buryatense. Appl. Environ. Microbiol. 81, 1775-1781 (2015).
- F. Chu, M. E. Lidstrom, XoxF acts as the predominant methanol dehydrogenase in the type I methanotroph Methylomicrobium buryatense. J. Bacteriol. 198, 1317-1325 (2016).
- A. Gilman et al., Bioreactor performance parameters for an industrially-promising methanotroph Methylomicrobium buryatense 5GB1. Microb. Cell Fact. 14, 182-189 (2015).
- K. Stone et al., Comparative study of oxygen-limited and methane-limited growth phenotypes of 23. Methylomicrobium buryatense 5GB1. Biochem. Eng. J. 161, 107707 (2020).
- I. R. Akberdin et al., Methane utilization in Methylomicrobium alcaliphilum 20^{ZR}: A systems approach, Sci. Rep. 8, 1-13 (2018).
- O. Ercan et al., Physiological and transcriptional responses of different industrial microbes at nearzero specific growth rates. Appl. Environ. Microbiol. 81, 5662-5670 (2015).
- T. Vos et al., Maintenance-energy requirements and robustness of Saccharomyces cerevisiae at aerobic near-zero specific growth rates. Microb. Cell Fact. 15, 1-20 (2016).
- Y. Fu, L. He, J. Reeve, D. A. C. Beck, M. E. Lidstrom, Core metabolism shifts during growth on methanol versus methane in the methanotroph Methylomicrobium buryatense 5GB1. MBio 10, 1-14 (2019).
- R. Khadka et al., Evolutionary history of copper membrane monooxygenases. Front. Microbiol. 9,
- E. F. Tentori, S. Fang, E. Richardson, RNA Biomarker trends across Type I and Type II aerobic methanotrophs in response to methane oxidation rates and transcriptome response to short-term methane and oxygen limitation in Methylomicrobium album BG8. Microbiol. Spectr. 8, e0000322 (2022).
- W. Overkamp et al., Physiological and cell morphology adaptation of Bacillus subtilis at near-zero specific growth rates: A transcriptome analysis. Environ. Microbiol. 17, 346-363 (2015).
- V. Hauryliuk, G. C. Atkinson, K. S. Murakami, T. Tenson, K. Gerdes, Recent functional insights into the 31. role of (p)ppGpp in bacterial physiology. *Nat. Rev. Microbiol.* **13**, 298–309 (2015).
- E. H. Wilson et al., A computational framework for identifying promoter sequences in nonmodel organisms using RNA-seq data sets. ACS Synth. Biol. 10, 1394-1405 (2021).
- Y. Yair et al., Cellular RNA targets of cold shock proteins CspC and CspE and their importance for 33
- serum resistance in septicemic Escherichia coli. mSystems 7, e0008622 (2022) P. Capy, G. Gasperi, C. Biémont, C. Bazin, Stress and transposable elements: Co-evolution or useful parasites? Heredity (Edinb). 85, 101-106 (2000).
- N. A. Sabnis, H. Yang, T. Romeo, Pleiotropic regulation of central carbohydrate metabolism in Escherichia coli via the gene csrA. J. Biol. Chem. 270, 29096-29104 (1995).
- H. La, J. P. A. Hettiaratchi, G. Achari, P. F. Dunfield, Biofiltration of methane. Bioresour. Technol. 268, 759-772 (2018).

- 37. M. Girard, A. A. Ramirez, G. Buelna, M. Heitz, Biofiltration of methane at low concentrations representative of the piggery industry-Influence of the methane and nitrogen concentrations. Chem. Eng. J. 168, 151-158 (2011).
- J. Nikiema, M. Girard, R. Brzezinski, M. Heitz, Biofiltration of methane using an inorganic filter bed: Influence of inlet load and nitrogen concentration. Can. J. Civ. Eng. 36, 1903-1910 (2009).
- N. Josiane, H. Michèle, The influence of the gas flow rate during methane biofiltration on an
- inorganic packing material. *Can. J. Chem. Eng.* **87**, 136–142 (2009). S. H. El Abbadi, E. D. Sherwin, A. R. Brandt, S. P. Luby, C. S. Criddle, Displacing fishmeal with protein derived from stranded methane. Nat. Sustain. 5, 47-56 (2022).
- F. D. Orata, J. P. Meier-Kolthoff, D. Sauvageau, L. Y. Stein, Phylogenomic analysis of the gammaproteobacterial methanotrophs (order methylococcales) calls for the reclassification of members at the genus and species levels. Front. Microbiol. 9, 1-17 (2018).
- A. W. Puri et al., Quorum sensing in a methane-oxidizing bacterium. J. Bacteriol. 199, e00773-16 (2017)
- J. W. Moon et al., Characterization of subsurface media from locations up- and down-gradient of a uranium-contaminated aquifer. Chemosphere 255, 126951 (2020).
- L. He, Y. Fu, M. E. Lidstrom, Quantifying methane and methanol metabolism of "Methylotuvimicrobium buryatense" 5GB1C under substrate limitation. mSystems **4**, 1–14 (2019).
- H. Li, R. Durbin, Fast and accurate short read alignment with Burrows-Wheeler transform. Bioinformatics 25, 1754-1760 (2009).
- H. Li et al., The Sequence Alignment/Map format and SAMtools. Bioinformatics 25, 2078-2079
- S. Anders, P. T. Pyl, W. Huber, HTSeq-A Python framework to work with high-throughput sequencing data. Bioinformatics 31, 166-169 (2015).
- A. Conesa et al., A survey of best practices for RNA-seq data analysis. Genome Biol. 17, 1-19 (2016).
- R. Sander, Compilation of Henry's law constants (version 4.0) for water as solvent. Atmos. Chem Phys. 15, 4399-4981 (2015). A. Ebrahim, J. A. Lerman, B. O. Palsson, D. R. Hyduke, COBRApy: CONstraints-based reconstruction
- and analysis for python. BMC Syst. Biol. 7, 74-79 (2013). K. T. Whiddon, R. Gudneppanavar, T. J. Hammer, D. A. West, M. C. Konopka, Fluorescence-based analysis of the intracytoplasmic membranes of type I methanotrophs. Microb. Biotechnol. 12,
- 1024-1033 (2019). R. Milo, R. Phillips, Cell Biology by the Numbers (Garland Science, ed. 1, 2015).
- L. He et al., A methanotrophic bacterium to enable methane removal for climate mitigation. NCBI GEO (Gene Expression Omnibus). https://www.ncbi.nlm.nih.gov/geo/query/acc. cgi?acc=GSE221011. Deposited 15 December 2022.

https://doi.org/10.1073/pnas.2310046120